

Quasiparticle and excitonic properties of monolayer SrTiO_3

Lorenzo Varrassi,^{*,†} Peitao Liu,[‡] and Cesare Franchini^{†,¶}

[†]*Dipartimento di Fisica e Astronomia, Università di Bologna, 40127 Bologna, Italy*

[‡]*Shenyang National Laboratory for Materials Science, Institute of Metal Research, Chinese Academy of Sciences, 110016 Shenyang, Liaoning, China*

[¶]*University of Vienna, Faculty of Physics and Center for Computational Materials Science, Kolingasse 14-16, A-1090, Vienna, Austria*

E-mail: lorenzo.varrassi3@unibo.it

Abstract

Strontium titanate SrTiO_3 is one of the most studied and paradigmatic transition metal oxides. Recently, a breakthrough has been achieved with the fabrication of freestanding SrTiO_3 ultrathin films down to the monolayer limit. However, the many-body effects on the quasiparticle and optical properties of monolayer SrTiO_3 remain unexplored. Using state-of-the-art many-body perturbation theory in the GW approximation combined with the Bethe-Salpeter equation, we study the quasiparticle band structure, optical and excitonic properties of monolayer SrTiO_3 . We show that quasiparticle corrections significantly alter the band structure topology; however, the widely used diagonal G_0W_0 approach yields unphysical band dispersions. The correct band dispersions are restored only by taking into account the off-diagonal elements of the self-energy. The optical properties are studied both in the optical limit and for finite momenta by computing the electron energy loss spectra. We find that the imaginary part of dielectric function at the long wavelength limit is dominated by three strongly bound excitonic peaks and the direct optical gap is associated to a bright exciton state with a large binding energy of 0.93 eV. We discuss the character of the excitonic peaks via the contributing interband transitions, and reveal that the lowest bound excitonic state becomes optical inactive for finite momenta along Γ -M, while the other two excitonic peaks disperse to higher energies and eventually merge for momenta close to M.

Transition Metal Oxide (TMO) perovskites have attracted wide interest in the last years due to the many intriguing physical properties and possible technological applications in various fields as oxide electronics, spintronic or catalysis.¹⁻⁴ Among them SrTiO_3 has acquired a prototypical role: it's one of the most studied perovskites and has been employed as a proving ground to propose or compare different computational schemes,^{5,6} including many-body *ab initio* methods⁷⁻¹¹ and machine-learning based algorithms.^{12,13} The role of its electronic structure in determining the conducting, magnetic and optical properties has been widely investigated, and intriguing phenomena such as superconductivity or two dimensional electron gas¹⁴⁻¹⁶ have been identified and analyzed. In particular recent theoretical works^{8-10,17} analyzed the role of electronic correlations and localized *d* states in the optical response, and highlighted how including an explicit description of excitonic

interactions is necessary to achieve a satisfactory agreement with the experimental data.

Recently, an important breakthrough has been achieved by Ji *et al.*¹⁸ through the synthesis of freestanding two-dimensional (2D) perovskites SrTiO_3 and BiFeO_3 films with a thickness reaching the monolayer limit. Their work proves that TMO perovskites films can be realized with thicknesses below the critical limit previously proposed as necessary for crystalline order stability.¹⁹ A year later freestanding PbTiO_3 films were fabricated with thicknesses down to four unit cells by Han *et al.*²⁰ In the last decades low-dimensional materials have attracted increasing attention due to their remarkable physical properties resulting from quantum confinement and reduced dimensionality effects, which differentiate them from bulk phases. In particular, 2D monolayer structures have been intensely studied due to their fascinating optical and excitonic physics: the enhanced electron-hole in-

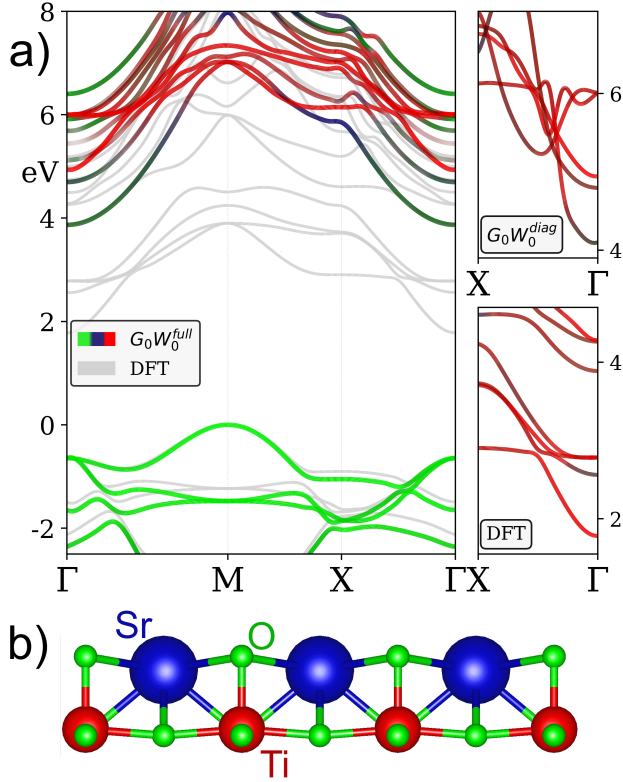


Figure 1: a) DFT (grey lines) and orbital-projected $G_0W_0^{full}$ band structures. Colors represent the O, Ti and Sr characters respectively. The two right panels show the orbital-projected unoccupied bands along X- Γ calculated by $G_0W_0^{diag}$ and DFT. b) Distorted monolayer SrTiO_3 structure.

interactions result in strongly bound excitons which dominate the optical response and charge transfer properties.^{21–32}

The experimental synthesis of freestanding TMO perovskites monolayers opens therefore the possibility of extending these analysis to SrTiO_3 . Nevertheless, to the best of our knowledge, the studies

Table 1: Direct and indirect QP and optical gaps for the monolayer SrTiO_3 , including the exciton binding energies E_{xc} of the first excitonic state in parentheses. Both $G_0W_0^{full}$ and $G_0W_0^{diag}$ predicted QP gaps are shown. The optical gaps and E_{xc} are determined by the solution of BSE starting from $G_0W_0^{full}$ predicted QP eigenstates.

	Direct (eV)	Indirect (eV)
BSE@ $G_0W_0^{full}(E_{xc})$	3.588 (0.93)	2.891 (0.98)
$G_0W_0^{full}$	4.514	3.870
$G_0W_0^{diag}$	4.743	4.099
DFT	2.427	1.781

of excitonic effect on this compound have been restricted to the bulk phase and thin films that do not reach the monolayer limit.

In this work we present a first-principles study of the optical spectra and the underlying excitonic transitions of monolayer SrTiO_3 , determined through the solution of the Bethe-Salpeter equation (BSE), where the quasiparticle (QP) eigenstates and screened Coulomb interactions are computed by the GW method. Our calculations indicate that DFT predicts incorrect hybridizations between Ti- d and O- $2p$ orbitals for the lower conduction bands and thus yields incorrect band characters. This leads to a severe failure for the diagonal G_0W_0 method when taking DFT one-electron energies and orbitals as a starting point. The correct band dispersions are restored only by taking into account the off-diagonal elements of the self-energy. We find that excitonic effects significantly alter the optical spectra. In addition to the spectral weight transfer visible also in bulk, new bound exciton peaks appear in monolayer SrTiO_3 . The origin of these excitonic peaks is clarified by analyzing the coupling components of the BSE eigenstates associated to these peaks. Moreover, we show that reduced dimensionality effects cause a considerable enhancement of exciton binding energies, yielding a binding energy as large as 0.93 eV for the first exciton at the optical direct gap.

Our calculations were performed using the VASP software,^{33,34} using a $24 \times 24 \times 1$ k-point mesh, a 600 eV cutoff energy for the wavefunctions and a 325 eV cutoff energy for the response functions. Finite basis errors on the QP energies were corrected by introducing a scissor operator determined using the YAMBO software.^{35,36}

The geometry of monolayer SrTiO_3 (001) was determined through a structural optimization starting from the relaxed cubic bulk phase. The optimization results in distortions along the z axis (see Fig. 1b), in agreement with previous works:^{37,38} The Ti and Sr atoms are displaced toward the inner side, with a larger displacement associated to the Sr atom, corresponding to the C_{4v} symmetry group. The distortions give rise to a polarization perpendicular to the monolayer plane³⁸ (see Fig. 1), which was calculated to be $0.069 |e|\text{\AA}$ using the Berry Phase method.³⁹ This value is consistent with the one estimated by the approximated expression $\mathbf{P}_{tot} = \sum_i \Delta R_i Z_i^*$ (where ΔR_i are the atomic displacements and Z_i the Born effective

charges) which gives $0.062 |e|\text{\AA}$.

Electronic properties In order to obtain accurate optical properties, an accurate description of the QP band structures is indispensable.⁴⁰ Here, the QP band structures were computed using a many-body G_0W_0 method^{41–43} with the screened interaction W calculated by the random phase approximation (RPA) using DFT one-electron energies and orbitals. Two different G_0W_0 schemes are discussed through this work. The first is the widely used one-shot approach based on the diagonal approximation of the self-energy Σ (referred to as $G_0W_0^{diag}$), and the other one is the $G_0W_0^{full}$ approach where eigenvalues and orbitals are determined by diagonalizing an Hamiltonian constructed from the full dynamical self-energy matrix.^{44–47} Remarkably, the QP corrections for monolayer SrTiO₃ are not just rigid energy shifts, but rather prove to be k-point- and band- dependent. As displayed in Fig. 1, the DFT bandstructure shows markedly different conduction bands dispersion with respect to $G_0W_0^{full}$ predicted ones. This difference is connected to an inadequate description of orbital characters by DFT. In the DFT bandstructure (grey lines in Fig. 1a) the conduction manifolds are dominated by Ti-*d* states. By contrast, the conduction manifolds predicted by $G_0W_0^{full}$ exhibit a sizable hybridization between Ti-*d* and Sr and O-*p* states. In particular, the lowest conduction band possesses a considerable mixing of Sr states (up to $\sim 40\%$) and O-*p* (up to $\sim 20\%$) along Γ -M and X- Γ . The valence bands characters are unchanged between $G_0W_0^{full}$ and DFT and are clearly contributed by the O-*p* states. Moreover the QP valence bands can be successfully modeled using a typical scissor plus stretching correction. It is instructive to compare these results with the widely used diagonal G_0W_0 approximation. Since the $G_0W_0^{diag}$ method retains a pronounced starting point dependence,^{48–52} it is not so surprising that $G_0W_0^{diag}$ on top of the incorrect DFT band characters results in unphysical band dispersions and multiple crossings long X- Γ among the lower conduction bands (see Fig. 1a). The failure of $G_0W_0^{diag}$ originates from the neglect of off-diagonal matrix elements of the self-energy, a coupling that can hybridize the single particle states. Indeed, using the full self-energy operator correctly couples the single particle Kohn-Sham orbitals and restores the correct hybridizations, thus avoiding the multiple band crossings (see Fig. 1a). There-

fore, going beyond the diagonal approximation for the self-energy is paramount for a correct description of the band dispersions of monolayer SrTiO₃. We note in passing that similar behaviours have been observed in bulk topological insulators^{53,54} (in particular, Aguilera and coworkers⁵⁵ noted how in Sb₂Tb₃ and Bi₂Tb₃ unphysical band dispersions may arise for orbitals strongly affected by *GW* corrections) and materials with strong *p-d* hybridizations.^{56–59}

The fundamental quasiparticle bandgaps of monolayer SrTiO₃ are summarized in Table 1. The DFT fundamental bandgap is indirect, with the valence band maximum (VBM) at M and the conduction band minimum (CBM) at Γ , while the DFT direct gap is defined at Γ . Despite the strong effect of QP corrections, the $G_0W_0^{full}$ indirect and direct gaps are opened at the same *k*-points (Γ –M and Γ), and are equal to 4.514 eV and 3.870 eV respectively.

Optical and excitonic properties The optical response of monolayer SrTiO₃ is dominated by excitonic effects. The direct optical gap is associated to a large excitonic binding energy of 0.93 eV (see Table 1). This value is much larger than the one estimated for the bulk phase (~ 0.205 – 0.240 eV^{8,9,17}). This is a typical consequence of the screening environment of 2D materials.^{30,31,60}

The BSE predicted imaginary part of the dielectric function in Fig. 2 is dominated by two very intense and narrow peaks. This is in marked contrast to the one computed from the independent particle approximation, which exhibits a long absorption tail. The first narrow peak is located below the QP direct gap and is determined by the excitonic state Λ_1 . A low-intensity feature is visible at the optical direct gap and is associated to the lowest bound exciton Λ_0 , with a considerable redshift at the onset energy of ~ 1.0 eV. Λ_0 is related to a bright exciton, albeit with a very weak oscillator strength (less than 5% of Λ_1). The continuum region displays a single prominent structure, in the form of sharp peak (i.e. Λ_2 with strongest oscillator strength) plus a shoulder.

Now, we turn to the analysis of the fine structure of bound excitons in Fig. 3. The lowest state Λ_0 is doubly degenerate and weakly optically active, with a modest oscillator strength. The contributions to the excitonic wavefunction in reciprocal space $A_{\mathbf{k}vc}^{\Lambda_0}$ are predominantly localized at Γ and originate from optical transitions from the valence O-*p* states the CBM. The low oscillator strength

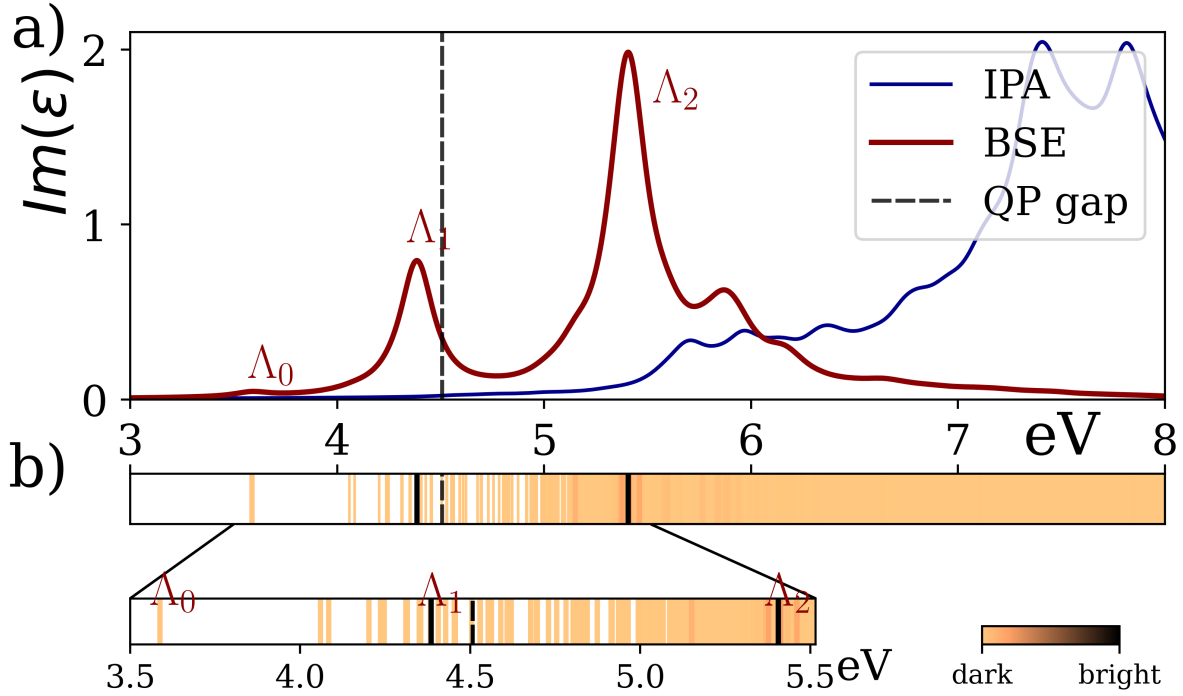


Figure 2: Imaginary part of dielectric functions with excitonic effects (BSE) and in the independent particle approximation (IPA). The vertical dashed line represents the fundamental direct gap. The BSE eigenvalue spectrum is given in b), with an insert zooming over the bound exciton region. The color coding indicates the associated oscillator strength with the maximum of the scale being set to that of Λ_2 .

can be explained in terms of orbital characters of the CBM. Specifically, the conduction band minimum retains a substantial O- p and Sr hybridization; in particular the Sr hybridization at Γ is mainly composed by Sr- s and Sr- p characters. This is in turn associated to a partial suppression of the optical matrix elements between the valence O- p states and the CBM.

The Λ_1 exciton is strongly bound, with an exciton binding energy of 1.31 eV. We note that the binding energy of the Λ_1 exciton here was determined as the difference between the BSE eigenvalue and the interband transition with the strongest contribution in the excitonic eigenstate, following Refs. ^{61,62} The major $A_{\mathbf{k}vc}^{\Lambda_1}$ terms correspond to interband transitions localized near Γ from the two highest valence bands formed by O- p_x/p_y states (doubly degenerate at Γ), to the second conduction band of Ti- d_{xy} character (see Fig. 3).

The BSE eigenstate $A_{\mathbf{k}vc}^{\Lambda_2}$ in the continuum mixes the (previously cited) O- $p_x/p_y \rightarrow$ Ti- d_{xy} optical transitions with a second excitation channel (highlighted with a different color in Fig. 3), from the O- p_z valence states to the non-dispersive conduction bands in the regions around $\Gamma - X$ and $\Gamma - M$ at ~ 6.0 eV, dominated by Ti- $d_{yz}/\text{Ti-}d_{xz}$ states

(with a negligible hybridization with other states, less than 12%).

The high intensity of the Λ_2 feature can be associated to the localization of the Ti- d states in the non-dispersive regions at ~ 6.0 eV. We note moreover that all O- p valence orbitals involved in Λ_1 and Λ_2 originate from the oxygen atoms situated in the Ti plane. Due to particular screening environment of 2D compounds, the orbitals perpendicular to the monolayer plane (e.g., the ones involved in the O- $p_z \rightarrow$ Ti- $d_{yz}/\text{Ti-}d_{xz}$ channel) experience a reduced screening with respect to the plane confined ones;⁶¹ this effect concurs to explain the large $\sim 2.0 - 2.1$ eV redshift of the Λ_2 peak.

Next, we turn to the investigation of the excitonic dispersion at finite \mathbf{q} , that is beyond the optical limit. This allows us to further characterize and discriminate the excitonic properties in 2D systems.^{63–67} The excitonic dispersion can be accessed experimentally by means of electron energy loss spectroscopy (EELS) or resonant inelastic x-ray spectroscopy (RIXS).⁶³ In particular in the EELS technique the cross section depends on the Loss function $L(\mathbf{q}, \omega) = -\text{Im}(\epsilon^{-1}(\mathbf{q}, \omega))$. Our computed Loss functions for various \mathbf{q} are

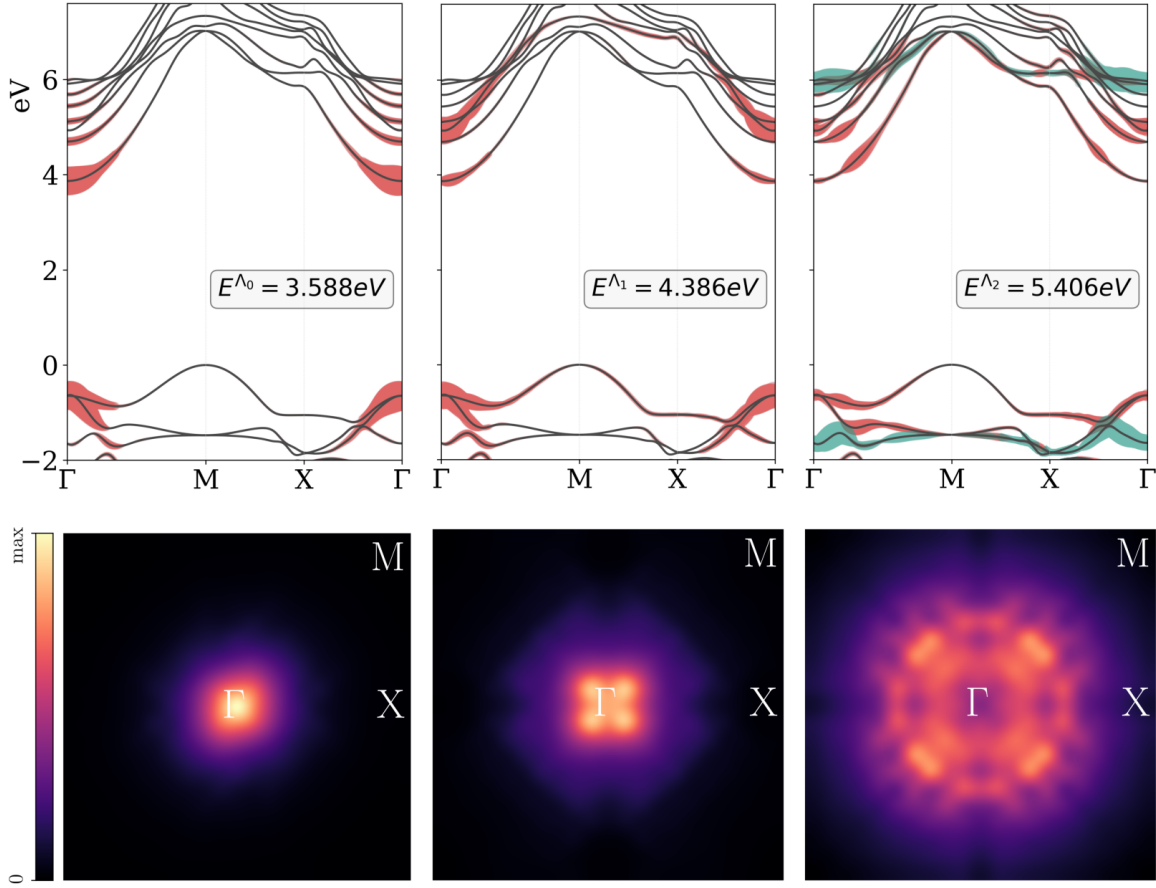


Figure 3: Upper panels: fatband analysis on the optical transitions associated with Λ_0 , Λ_1 and Λ_2 states. The fatness of the bands is proportional to the square of the amplitude of the electron-hole coupling coefficients $|A_{\mathbf{k}vc}^\Lambda|^2$ with v , c , \mathbf{k} and Λ denoting the valence band index, conduction band index, k -point and BSE eigenvalue, respectively. For Λ_2 , the $O-p \rightarrow \text{Ti-}d_{yz} + \text{Ti-}d_{xz}$ optical transitions, discussed in the text, are highlighted by a light blue color. Lower panels: Distribution of the BSE eigenvectors in the Brillouin zone for the corresponding BSE eigenvalues. The color coding denotes $\sum_{v,c} |A_{\mathbf{k}vc}^\Lambda|^2$.

plotted in Fig. 4 along $\Gamma - M$ (corresponding to the indirect gap direction).

It's interesting to find that the doubly degenerate lowest excitonic state Λ_0 , that yields a low-intensity feature for $q \rightarrow 0$, becomes completely optically inactive along Γ -M. Furthermore, the analysis of exciton dispersions (insert in Fig. 4) shows that the double-degeneracy is splitted away from Γ , and the two resulting excitonic bands reach their minimum at $\mathbf{q} = M$, in correspondence of the indirect QP bandgap. The lowest (dark) excitonic band shows a parabolic dispersion around M , with an associated binding energy of 0.98 eV at M .

Upon increasing momentum transfer, the peak associated with the Λ_1 state disperses to higher energies and progressively merges with the high-intensity structure at ~ 5.5 eV (identifiable with the Λ_2 transition). At large \mathbf{q} a new feature ap-

pears at transition energies around 4.1 eV, which originates from the interband transitions from the three highest valence bands to the lowest conduction band. In particular, for $\mathbf{q} = M$ a non-negligible contribution to the BSE eigenstate $A_{v\mathbf{c}\mathbf{k}}(\mathbf{q} = M)$ (up to 30% of the total spectral weight) is obtained by the transitions from valence $O-p_z$ states, which are also involved also in the Λ_2 excitonic transition.

In summary, we have investigated the quasiparticle and excitonic properties of freestanding monolayer SrTiO_3 , using an *ab initio* approach based on many body perturbation GW theory and Bethe-Salpeter equation. We demonstrate that the inclusion of off-diagonal self-energy matrix elements in the G_0W_0 scheme is crucial to correctly describe the strong hybridization of the lower conduction bands (which

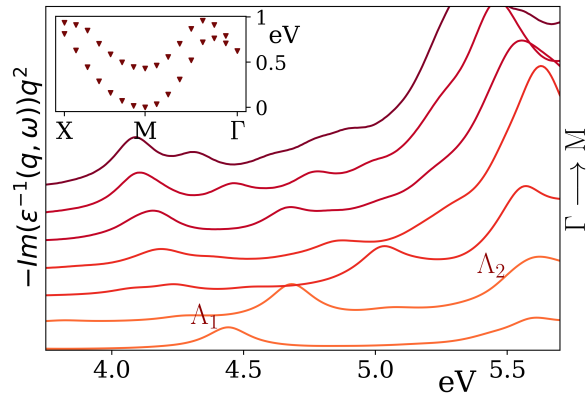


Figure 4: Loss function for transferred momenta along the high-symmetry direction Γ -M, from $\mathbf{q} = \text{M}/8$ to $\mathbf{q} = \text{M}$. Each curve is multiplied by q^2 , following Cudazzo and coworkers.^{63,64} The insert shows the excitonic band structure for the lowest two excitons along $\text{X} - \text{M} - \Gamma$; the zero energy is set at the eigenvalues minimum at M.

is wrongly accounted for by DFT) and hence prevents the appearance of unphysical dispersions.

The excitonic properties both in the optical limit $\mathbf{q} \rightarrow 0$ and for finite momenta have been studied. We find that the spectra at $\mathbf{q} \rightarrow 0$ is dominated by excitonic effects, with a large binding energy of ~ 0.93 eV at the direct optical gap. The analysis of the BSE coupling components shows that the most intense peaks are originated from the $\text{O}-p \rightarrow \text{Ti}-d$ interband transitions, in conformity with the bulk description. In particular, the transitions from the in-plane $\text{O}-p_x/p_y$ orbitals to $\text{Ti}-d_{xy}$ orbitals and from out-of-plane $\text{O}-p_z$ orbitals to $\text{Ti}-d_{xz}/d_{yz}$ orbitals form separate excitation channels, which allows us to differentiate the two peaks. At finite \mathbf{q} , the lowest exciton becomes inactive with a parabolic excitonic dispersion around the transition minimum at $\mathbf{q} = \text{M}$, an energy lower than the direct optical gap.

Our work opens a path in exploring the excitonic properties of 2D TMO perovskites and sets the basis for on-going and future experimental and computational studies on ultrathin materials.

Acknowledgement

The authors thank G. Kresse, M. Marsili and J. He for fruitful discussions. The computational results have been achieved using the Vienna Scientific Cluster (VSC) and the Galileo100 cluster (CINECA, LIMIT project).

References

- (1) Dogan, F.; Lin, H.; Guilloux-Viry, M.; Peña, O. Focus on properties and applications of perovskites. *Science and Technology of Advanced Materials* **2015**, *16*, 020301.
- (2) Guan, X.; Guo, L. Cocatalytic Effect of SrTiO_3 on Ag_3PO_4 toward Enhanced Photocatalytic Water Oxidation. *ACS Catalysis* **2014**, *4*, 3020–3026.
- (3) Liu, Y.; Xie, L.; Li, Y.; Yang, R.; Qu, J.; Li, Y.; Li, X. Synthesis and high photocatalytic hydrogen production of SrTiO_3 nanoparticles from water splitting under UV irradiation. *Journal of Power Sources* **2008**, *183*, 701–707.
- (4) Shoji, S.; Yin, G.; Nishikawa, M.; Atarashi, D.; Sakai, E.; Miyauchi, M. Photocatalytic reduction of CO_2 by Cu_xO nanocluster loaded SrTiO_3 nanorod thin film. *Chemical Physics Letters* **2016**, *658*, 309–314.
- (5) Betzinger, M.; Friedrich, C.; Görling, A.; Blügel, S. Precise response functions in all-electron methods: Application to the optimized-effective-potential approach. *Phys. Rev. B* **2012**, *85*, 245124.
- (6) Ekuma, C. E.; Jarrell, M.; Moreno, J.; Bagayoko, D. First principle electronic, structural, elastic, and optical properties of strontium titanate. *AIP Advances* **2012**, *2*, 012189.
- (7) Cappellini, G.; Bouette-Russo, S.; Amadon, B.; Noguera, C.; Finocchi, F. Structural properties and quasiparticle energies of cubic SrO , MgO and SrTiO_3 . *Journal of Physics: Condensed Matter* **2000**, *12*, 3671.
- (8) Varrassi, L.; Liu, P.; Yavas, Z. E.; Bokdam, M.; Kresse, G.; Franchini, C. Optical and excitonic properties of transition metal

- oxide perovskites by the Bethe-Salpeter equation. *Phys. Rev. Materials* **2021**, *5*, 074601
- (9) Sponza, L.; Vénard, V.; Sottile, F.; Giorgetti, C.; Reining, L. Role of localized electrons in electron-hole interaction: The case of SrTiO₃. *Phys. Rev. B* **2013**, *87*, 235102
- (10) Gogoi, P. K.; Sponza, L.; Schmidt, D.; Asmara, T. C.; Diao, C.; Lim, J. C. W.; Poh, S. M.; Kimura, S.-i.; Trevisanutto, P. E.; Olevano, V.; Rusydi, A. Anomalous excitons and screenings unveiling strong electronic correlations in SrTi_{1-x}Nb_xO₃ ($0 \leq x \leq 0.005$). *Phys. Rev. B* **2015**, *92*, 035119
- (11) Ergönenc, Z.; Kim, B.; Liu, P.; Kresse, G.; Franchini, C. Converged GW quasiparticle energies for transition metal oxide perovskites. *Phys. Rev. Mater.* **2018**, *2*, 024601
- (12) Tröster, A.; Verdi, C.; Dellago, C.; Rychetsky, I.; Kresse, G.; Schranz, W. Hard antiphase domain boundaries in strontium titanate unravelled using machine-learned force fields. *Phys. Rev. Materials* **2022**, *6*, 094408
- (13) Verdi, C.; Ranalli, L.; Franchini, C.; Kresse, G. Quantum paraelectricity and structural phase transitions in strontium titanate beyond density functional theory. *Phys. Rev. Materials* **2023**, accepted
- (14) Santander-Syro, A. F. et al. Two-dimensional electron gas with universal subbands at the surface of SrTiO₃. *Nature* **2011**, *469*, 189–193
- (15) Wang, Z.; Zhong, Z.; Hao, X.; Gerhold, S.; Stöger, B.; Schmid, M.; Sánchez-Barriga, J.; Varykhalov, A.; Franchini, C.; Held, K.; Diebold, U. Anisotropic two-dimensional electron gas at SrTiO₃(110). *Proceedings of the National Academy of Sciences* **2014**, *111*, 3933–3937
- (16) Meevasana, W.; King, P. D. C.; He, R. H.; Mo, S.-K.; Hashimoto, M.; Tamai, A.; Songsiriritthigul, P.; Baumberger, F.; Shen, Z.-X. Creation and control of a two-dimensional electron liquid at the bare SrTiO₃ surface. *Nature Materials* **2011**, *10*, 114–118
- (17) Begum, V.; Gruner, M. E.; Pentcheva, R. Role of the exchange-correlation functional on the structural, electronic, and optical properties of cubic and tetragonal SrTiO₃ including many-body effects. *Phys. Rev. Materials* **2019**, *3*, 065004
- (18) Ji, D. et al. Freestanding crystalline oxide perovskites down to the monolayer limit. *Nature* **2019**, *570*, 87–90
- (19) Hong, S. S.; Yu, J. H.; Lu, D.; Marshall, A. F.; Hikita, Y.; Cui, Y.; Hwang, H. Y. Two-dimensional limit of crystalline order in perovskite membrane films. *Science Advances* **2017**, *3*, eaao5173
- (20) Han, L.; Fang, Y.; Zhao, Y.; Zang, Y.; Gu, Z.; Nie, Y.; Pan, X. Giant Uniaxial Strain Ferroelectric Domain Tuning in Freestanding PbTiO₃ Films. *Advanced Materials Interfaces* **2020**, *7*, 1901604
- (21) Haug, H.; Koch, S. W. *Quantum Theory of the Optical and Electronic Properties of Semiconductors*, 5th ed.; WORLD SCIENTIFIC, 2009
- (22) Qiu, D. Y.; da Jornada, F. H.; Louie, S. G. Optical Spectrum of MoS₂: Many-Body Effects and Diversity of Exciton States. *Phys. Rev. Lett.* **2013**, *111*, 216805
- (23) Sponza, L.; Amara, H.; Attacalite, C.; Latil, S.; Galvani, T.; Paleari, F.; Wirtz, L.; Ducastelle, F. m. c. Direct and indirect excitons in boron nitride polymorphs: A story of atomic configuration and electronic correlation. *Phys. Rev. B* **2018**, *98*, 125206

- (24) Qiu, D. Y.; da Jornada, F. H.; Louie, S. G. Screening and many-body effects in two-dimensional crystals: Monolayer MoS₂. *Phys. Rev. B* **2016**, *93*, 235435
- (25) Yang, L.; Deslippe, J.; Park, C.-H.; Cohen, M. L.; Louie, S. G. Excitonic Effects on the Optical Response of Graphene and Bilayer Graphene. *Phys. Rev. Lett.* **2009**, *103*, 186802
- (26) Fugallo, G.; Cudazzo, P.; Gatti, M.; Sottile, F. Exciton band structure of molybdenum disulfide: from monolayer to bulk. *Electronic Structure* **2021**, *3*, 014005
- (27) Ekuma, C. E. Optical absorption in monolayer SnO₂. *Phys. Rev. B* **2019**, *99*, 075421
- (28) Cudazzo, P.; Sponza, L.; Giorgetti, C.; Reining, L.; Sottile, F.; Gatti, M. Exciton Band Structure in Two-Dimensional Materials. *Phys. Rev. Lett.* **2016**, *116*, 066803
- (29) Wang, G.; Chernikov, A.; Glazov, M. M.; Heinz, T. F.; Marie, X.; Amand, T.; Urbaszek, B. Colloquium: Excitons in atomically thin transition metal dichalcogenides. *Rev. Mod. Phys.* **2018**, *90*, 021001
- (30) Hüser, F.; Olsen, T.; Thygesen, K. S. How dielectric screening in two-dimensional crystals affects the convergence of excited-state calculations: Monolayer MoS₂. *Phys. Rev. B* **2013**, *88*, 245309
- (31) Chernikov, A.; Berkelbach, T. C.; Hill, H. M.; Rigosi, A.; Li, Y.; Aslan, B.; Reichman, D. R.; Hybertsen, M. S.; Heinz, T. F. Exciton Binding Energy and Nonhydrogenic Rydberg Series in Monolayer WS₂. *Phys. Rev. Lett.* **2014**, *113*, 076802
- (32) Guilhon, I.; Marques, M.; Teles, L. K.; Palummo, M.; Pulci, O.; Botti, S.; Bechstedt, F. Out-of-plane excitons in two-dimensional crystals. *Phys. Rev. B* **2019**, *99*, 161201
- (33) Kresse, G.; Furthmüller, J. Efficient iterative schemes for ab initio total-energy calculations using a plane-wave basis set. *Phys. Rev. B* **1996**, *54*, 11169–11186
- (34) Kresse, G.; Furthmüller, J. Efficiency of ab-initio total energy calculations for metals and semiconductors using a plane-wave basis set. *Computational Materials Science* **1996**, *6*, 15–50
- (35) Marini, A.; Hogan, C.; Grüning, M.; Varsano, D. yambo: An ab initio tool for excited state calculations. *Computer Physics Communications* **2009**, *180*, 1392–1403
- (36) Sangalli, D. et al. Many-body perturbation theory calculations using the yambo code. *Journal of Physics: Condensed Matter* **2019**, *31*, 325902
- (37) Pan, H.; Zhang, Y.; Jia, H.; Cao, E.; Yang, Z. Electronic Structures, Stabilities, and Magnetism of SrTiO₃ Monolayer and Ultrathin Nanotubes. *Journal of Superconductivity and Novel Magnetism* **2021**, *34*, 2093–2104
- (38) Xiao, X.-B.; Liu, B.-G. Freestanding perovskite oxide monolayers as two-dimensional semiconductors. *Nanotechnology* **2021**, *32*, 145705
- (39) King-Smith, R. D.; Vanderbilt, D. Theory of polarization of crystalline solids. *Phys. Rev. B* **1993**, *47*, 1651–1654
- (40) Liu, P.; Franchini, C. Advanced First-Principle Modeling of Relativistic Ruddlesden–Popper Strontium Iridates. *Applied Sciences* **2021**, *11*
- (41) Hybertsen, M. S.; Louie, S. G. Electron correlation in semiconductors and insulators:

- Band gaps and quasiparticle energies. *Phys. Rev. B* **1986**, *34*, 5390–5413
- .
- (42) Shishkin, M.; Kresse, G. Implementation and performance of the frequency-dependent *GW* method within the PAW framework. *Phys. Rev. B* **2006**, *74*, 035101
- .
- (43) Shishkin, M.; Kresse, G. Self-consistent *GW* calculations for semiconductors and insulators. *Phys. Rev. B* **2007**, *75*, 235102
- .
- (44) Shishkin, M.; Marsman, M.; Kresse, G. Accurate Quasiparticle Spectra from Self-Consistent *GW* Calculations with Vertex Corrections. *Phys. Rev. Lett.* **2007**, *99*, 246403
- .
- (45) van Schilfgaarde, M.; Kotani, T.; Faleev, S. Quasiparticle Self-Consistent *GW* Theory. *Phys. Rev. Lett.* **2006**, *96*, 226402
- .
- (46) Faleev, S. V.; van Schilfgaarde, M.; Kotani, T. All-Electron Self-Consistent *GW* Approximation: Application to Si, MnO, and NiO. *Phys. Rev. Lett.* **2004**, *93*, 126406
- .
- (47) Reining, L. The *GW* approximation: content, successes and limitations. *WIREs Computational Molecular Science* **2018**, *8*, e1344
- .
- (48) Onida, G.; Reining, L.; Rubio, A. Electronic excitations: density-functional versus many-body Green’s-function approaches. *Rev. Mod. Phys.* **2002**, *74*, 601–659
- .
- (49) Golze, D.; Dvorak, M.; Rinke, P. The *GW* Compendium: A Practical Guide to Theoretical Photoemission Spectroscopy. *Frontiers in Chemistry* **2019**, *7*
- .
- (50) Delaney, K.; García-González, P.; Rubio, A.; Rinke, P.; Godby, R. W. Comment on “Band-Gap Problem in Semiconductors Revisited: Effects of Core States and Many-Body Self-Consistency”. *Phys. Rev. Lett.* **2004**, *93*, 249701
- .
- (51) Fuchs, F.; Furthmüller, J.; Bechstedt, F.; Shishkin, M.; Kresse, G. Quasiparticle band structure based on a generalized Kohn-Sham scheme. *Phys. Rev. B* **2007**, *76*, 115109
- .
- (52) Klimeš, J.; Kresse, G. Kohn-Sham band gaps and potentials of solids from the optimised effective potential method within the random phase approximation. *The Journal of Chemical Physics* **2014**, *140*, 054516
- .
- (53) Aguado-Puente, P.; Fahy, S.; Grüning, M. *GW* study of pressure-induced topological insulator transition in group-IV tellurides. *Phys. Rev. Research* **2020**, *2*, 043105
- .
- (54) Aguilera, I.; Friedrich, C.; Blügel, S. Many-body corrected tight-binding Hamiltonians for an accurate quasiparticle description of topological insulators of the Bi₂Se₃ family. *Phys. Rev. B* **2019**, *100*, 155147
- .
- (55) Aguilera, I.; Friedrich, C.; Bihlmayer, G.; Blügel, S. *GW* study of topological insulators Bi₂Se₃, Bi₂Te₃, and Sb₂Te₃: Beyond the perturbative one-shot approach. *Phys. Rev. B* **2013**, *88*, 045206
- .
- (56) Nabok, D.; Blügel, S.; Friedrich, C. Electron-plasmon and electron-magnon scattering in ferromagnets from first principles by combining *GW* and *GT* self-energies. *npj Computational Materials* **2021**, *7*, 178
- .
- (57) van Schilfgaarde, M.; Kotani, T.; Faleev, S. V. Adequacy of approximations in *GW* theory. *Phys. Rev. B* **2006**, *74*, 245125
- .
- (58) Aguilera, I.; Palacios, P.; Wahnón, P. Understanding Ti intermediate-band formation in partially inverse thiospinel MgIn₂S₄ through many-body approaches. *Phys. Rev. B* **2011**, *84*, 115106
- .

- (59) Gatti, M.; Bruneval, F.; Olevano, V.; Reining, L. Understanding Correlations in Vanadium Dioxide from First Principles. *Phys. Rev. Lett.* **2007**, *99*, 266402 .
- (60) Cudazzo, P.; Tokatly, I. V.; Rubio, A. Dielectric screening in two-dimensional insulators: Implications for excitonic and impurity states in graphane. *Phys. Rev. B* **2011**, *84*, 085406 .
- (61) Yu, H.; Laurien, M.; Hu, Z.; Rubel, O. Exploration of the bright and dark exciton landscape and fine structure of MoS₂ using G₀W₀-BSE. *Phys. Rev. B* **2019**, *100*, 125413 .
- (62) Antonius, G.; Qiu, D. Y.; Louie, S. G. Orbital Symmetry and the Optical Response of Single-Layer MX Monochalcogenides. *Nano Letters* **2018**, *18*, 1925–1929 .
- (63) Cudazzo, P.; Sponza, L.; Giorgetti, C.; Reining, L.; Sottile, F.; Gatti, M. Exciton Band Structure in Two-Dimensional Materials. *Phys. Rev. Lett.* **2016**, *116*, 066803 .
- (64) Bonacci, M.; Zanfagnini, M.; Molinari, E.; Ruini, A.; Caldas, M. J.; Ferretti, A.; Varsano, D. Excitonic effects in graphene-like C₃N. *Phys. Rev. Mater.* **2022**, *6*, 034009 .
- (65) Fugallo, G.; Cudazzo, P.; Gatti, M.; Sottile, F. Exciton band structure of molybdenum disulfide: from monolayer to bulk. *Electronic Structure* **2021**, *3*, 014005 .
- (66) Qiu, D. Y.; Cao, T.; Louie, S. G. Non-analyticity, Valley Quantum Phases, and Lightlike Exciton Dispersion in Monolayer Transition Metal Dichalcogenides: Theory and First-Principles Calculations. *Phys. Rev. Lett.* **2015**, *115*, 176801 .
- (67) Sponza, L.; Amara, H.; Attaccalite, C.; Latil, S.; Galvani, T.; Paleari, F.; Wirtz, L.; Ducastelle, F. m. c. Direct and indirect excitons in boron nitride polymorphs: A story of atomic configuration and electronic correlation. *Phys. Rev. B* **2018**, *98*, 125206 .